Fully Additive Electrohydrodynamic Inkjet-Printed TiO$_2$ Mid-Infrared Meta-Optics

Holly J. C. Brunner,* James Whitehead, Ricky Gibson, Joshua R. Hendrickson, Arka Majumdar, and J. Devin MacKenzie*

Additive manufacturing at the micron and sub-micron scale is a rapidly expanding field with electrohydrodynamic inkjet (EHDIJ) printing proving to be a critical fabrication technique that will enable continued advancement. Increasing the range of materials that can be used with EHDIJ printing to create micron and sub-micron scale features is critical for increasing the variety of devices that can be fabricated with this method. Ceramic, semiconducting, and hybrid organic–inorganic materials are essential for meta-optics and micro-electromechanical systems devices, yet these materials are vastly underexplored for applications in EHDIJ printing. A novel printing solution is presented containing a titania alkoxide precursor that is compatible with EHDIJ printing and capable of producing final printed features of 1 μm and below; the highest resolution features ever reported for this family of materials and this method. This solution is used to fabricate the first EHDIJ printed and functioning mid-infrared meta-optics lens, capable of focusing 5 μm light.

1. Introduction

The past two decades have seen significant research and development efforts toward additive manufacturing of functional materials using inkjet printing and direct-write 3D printing techniques for applications such as displays and flexible electronics.[1,2,3] In the case of traditional inkjet printing, fluid surface energy constraints make it difficult for this technique to reach below the picoliter droplet size and 10 μm printed feature size regime without the use of additional patterning. Extrusion or filament-based 3D printing requires contact between the nozzle, extruded material, and substrate to facilitate printing. Without additional processing, this limits the printing resolution to the nozzle diameter or larger, depending on the material.[4,5] Electrohydrodynamic inkjet printing (EHDIJ) is a rapidly advancing fabrication technique used to additively print functional materials with micron and submicron precision. This method uses an applied electric field between the printing nozzle and the substrate stage to create the necessary fluid flow to enable printing.[6] EHDIJ can produce directed femtoliter size droplets from solution-borne functional materials with a broader range of viscosities than conventional, pressure-actuated inkjet printing by using an applied electric field on polarizable fluids to overcome energetic barriers to smaller droplet formation. In contrast to extrusion 3D printing, EHDIJ is a noncontact printing technique. The space between the printing nozzle and the substrate facilitates solvent evaporation of the ejected drop, reducing the volume prior to contact with the substrate.[4] Coupled with optimally engineered materials, EHDIJ printing can provide many benefits over traditional micron-scale fabrication techniques, including large area photolithography, two-photon resist direct-write lithography, and electron beam lithography.[6,7] While lithographic techniques can achieve very high resolution and good reproducibility, they are typically indirect or subtractive and pattern transfer is done with an intermediate, sacrificial material, not the final product. In most cases, the processing produces significant waste fractions and is challenging and expensive to scale to a large area and high-volume manufacturing. Here we propose a fully additive process for direct pattern deposition of high refractive index, functional optical materials and demonstrate its efficacy via creating a metalens at the mid-infrared wavelength.

The EHDIJ techniques and materials present a unique combination of benefits, including rapid prototyping and fabrication, maskless lithography, ambient condition fabrication, and a wider range of material types including metal salt[8] and metal nanoparticle based inks,[4] carbon nanotube, and graphene inks, conductive polymers,[9] photopolymers,[10] and many other varieties of materials in a range of viscosity from less than 10 centipoise (cP)[11] to at least 5000 cP.[10,12] Additionally, most EHDIJ printed devices can be fabricated without the assistance of

H. J. C. Brunner, J. D. MacKenzie
Materials Science and Engineering Department
University of Washington
Seattle, WA 98195, USA
E-mail: hjcb2@uw.edu; jdmacken@uw.edu

J. Whitehead, A. Majumdar
Department of Electrical and Computer Engineering
University of Washington
Seattle, WA 98195, USA

R. Gibson, J. R. Hendrickson
Air Force Research Laboratory
Sensors Directorate
2241 Avionics Circle, Wright-Patterson AFB, OH 45433, USA

J. D. MacKenzie
Mechanical Engineering Department
University of Washington
Seattle, WA 98195, USA

**ADVANCED
SCIENCE NEWS**
www.advancedsciencenews.com

**ADVANCED
MATERIALS
INTERFACES**
www.advmatinterfaces.de

chemical etchants, thus reducing overall resource use and toxic effluents from the process.[11] EHDIJ printing techniques have already been used to successfully print a wide range of materials; however, much of the focus in the field, including the reported highest resolution printed features, involved metal nanoparticle inks or UV-curable polymers.[7,10] There has been significantly less emphasis on materials and process development for EHDIJ printed ceramics and inorganic–organic hybrid materials.

Ceramic and semiconducting materials, such as TiO_2, are of particular interest for applications in meta-optics,[13,14] and micro-electromechanical systems (MEMS) devices due to the optimal combination of material properties such as a high refractive index,[15,16] low absorption over a broad wavelength range, including the visible, near-infrared, and mid-infrared spectrum,[17] low signal losses, increased efficiencies,[14] and mechanical and thermal robustness. As such, there is significant motivation to develop high-resolution printable ceramics to bring the benefits of printed electronics to optical devices and MEMS. Previous work by Lewis et al. used an extrusion-based 3D printer to print a very high viscosity TiO_2 alkoxide precursor and polymer filament to fabricate structures with possible optical device applications. This process, however, requires a sacrificial layer to enable post-printing sintering and condensation to achieve their final reported minimum feature size of 268 ± 9 nm.[18] This significantly limits the types of structures and devices that can be printed and is not appropriate for meta-optical lenses, which rely on 2D arrays of sub-wavelength structures. These scatterer structures must remain well adhered to the substrate and maintain the optimal pitch to focus light.[19] As such, a novel process and printing solution need to be developed to create a viable fabrication method to achieve fully printed meta-optics.

The meta-optics pattern for this project was designed around the principles of subwavelength diffractive optics. Under this mechanism, the desired phase shift in light occurs by exploiting variations in the lateral size and orientation of the individual scatterers while maintaining a uniform thickness.[20] The scatterers must have a subwavelength quasiperiodic structure with respect to the wavelength the metalens is designed to focus. The results are optical elements that are substantially thinner than a conventional diffractive lens, typically less than the wavelength of the focused beam. Furthermore, these principles have been used to fabricate metalenses with a large numerical aperture (NA > 0.99), indicating a very small spot size of the focused light and increased resolving capabilities.[21,22] This has benefits in the ever-expanding internet of things, which relies on a large network of thin and inexpensive sensors, optical displays as well as other emerging technologies that require lightweight optical components.[20,21] Previous work focused on EHDIJ printed micro and nanolens arrays by Lianqing Liu et. al used UV-curable polymers as the printed materials. These materials have a lower refractive index and higher absorption at $\lambda = 5$ μm than is optimal for maximum lensing efficiency.[10,14,21–23] Furthermore, these printing experiments examine the lensing capabilities of the individual printed feature based on conventional diffractive lens designs, not the subwavelength diffractive optics of a meta-optics lens demonstrated in this body of work.[10,23]

This paper reports the first fully additive EHDIJ printed mid-infrared meta-optics lens made from a functional TiO_2 alkoxide and polyvinyl pyrrolidone (PVP) hybrid ink. Printing

resolutions of sub-1μm have been demonstrated and waveform-driven control of individual femtoliter-scale precursor ink droplets has been used to fully-additively print a functional meta-optic lens designed to focus 5 μm light. This represents a step forward in additive manufacturing toward the scalable nanomanufacturing of photonics.

2. Methods

The printing solution used to make the metaoptical structures is made from ethylene glycol (EG), titanium diisopropoxide bis(acetylacetonate) (75% in isopropyl alcohol), polyvinylpyrrolidone (≈55 000 mw) (PVP), isopropyl alcohol (IPA), and poly(melamine-co-formaldehyde) methylated, a thermally induced crosslinking agent. The 1 mm × 1 mm meta-optical lenses are fabricated on an n-type silicon wafer. The substrate is coated with trichloro(1H, 1H, 2H, 2H-perfluorooctyl)silane, a hydrophobic, self-assembling monolayer (SAM) in order to increase the contact angle of the printed solution. Under ambient conditions, the metasurface was printed on the SAM coated substrate, using an electrohydrodynamic inkjet (EHDIJ) printer made by SIJ Technology. **Figure 1**a,b shows a schematic of the EHDIJ printer setup. Figure 1c,d shows the contact angle between the TiO_2 precursor printing solution and the Si substrate, with Figure 1c showing the ink on a clean Si wafer without the hydrophobic SAM and Figure 1d showing the contact angle on a clean Si wafer coated with the hydrophobic SAM. The presence of trichloro(1H, 1H, 2H, 2H-perfluorooctyl) changes the contact angle between the printing solution and the silicon substrate from total wetting (contact angle ≈0°) to a high contact angle of 68°. Figure 1e shows an example of the TiO_2 printing solution EHDIJ printed on an uncoated Si wafer and Figure 1f shows the same solution printed on the hydrophobic SAM coated Si wafer. Both examples were printed using the continuous mode of the EHDIJ printer. In this mode, the EHDIJ printer maintains a set applied voltage between the gold filament inside the printer nozzle and the substrate and maintains a set waveform, with the spacing of each drop predominantly determined by the printer stage speed. The printer can also run in dropwise mode. In this mode, the printer turns the parameters on and off at discrete points set by the print pattern script. The printer has stage movement control down to 1 μm.

For additive printing of complex meta-optical structures, it is essential to use a process with precise control over the location and volume of the deposited material. In EHDIJ, the method of continuously printing a solution can result in submicron printed features, but the method does not provide the level of drop size and location precision necessary to fabricate a quasiperiodic meta-optics lens. The dropwise EHDIJ printing method uses point-by-point control of printing parameters. In this mode, the location and pitch of each drop are controlled by pausing droplet ejection during discrete stage movements before resuming ink flow at a defined location. The volume of the ejected drop is controlled by the parameters set at each point. As we demonstrate here, a digital dropwise EHDIJ method can provide the degree of material deposition control necessary to print meta-optics patterns with any level of periodicity where the deposited droplet location depends primarily on the translational
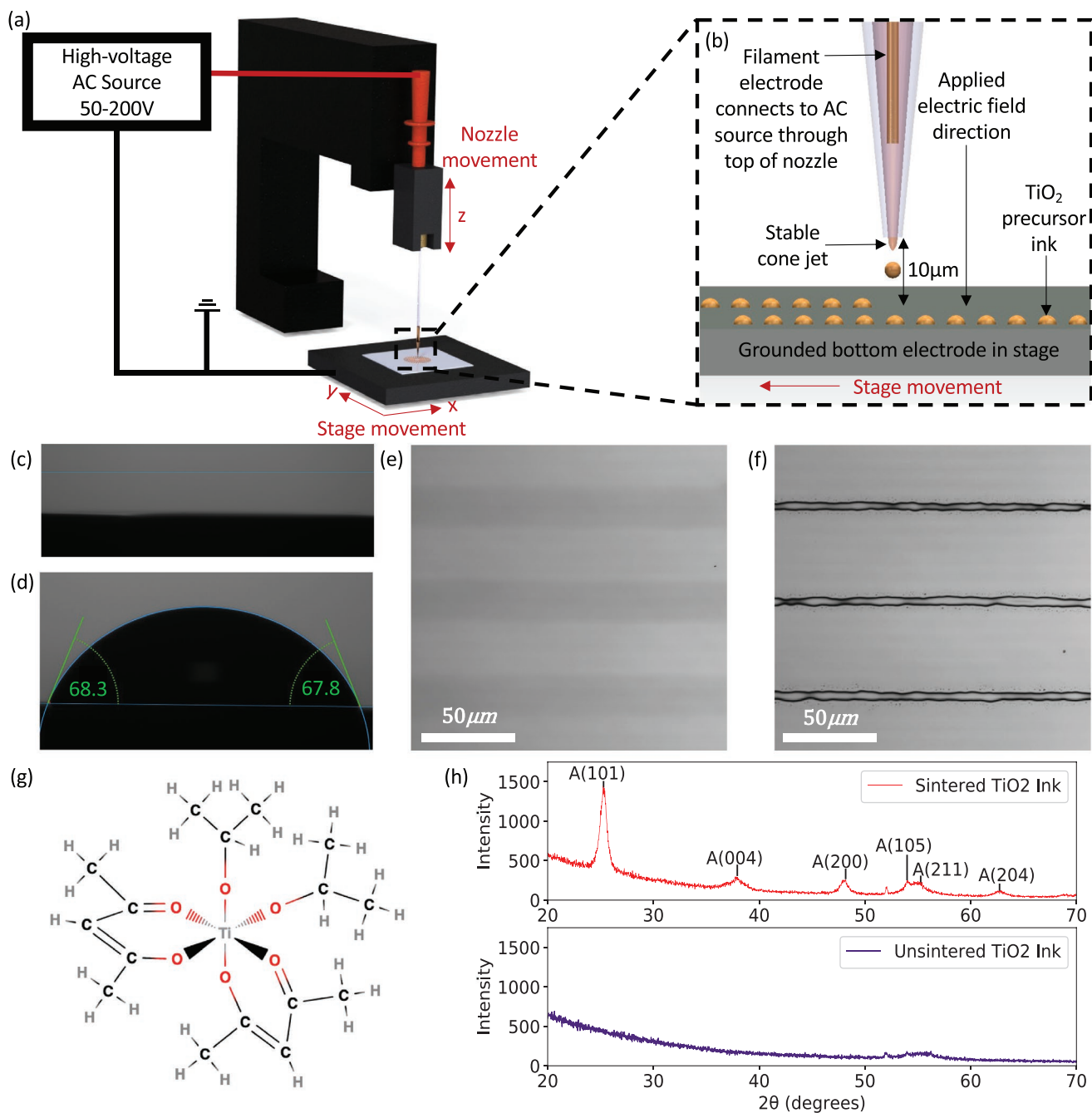
Figure 1. a) Wide-view schematic of EHDIJ printing setup. b) Close-up schematic of EHDIJ printing nozzle and substrate. c) Contact angle of TiO$_2$ precursor printing solution on clean Si substrate without the hydrophobic self-assembled monolayer coating to decrease droplet spreading and increase printing resolution. d) Contact angle of TiO$_2$ precursor printing solution on clean Si substrate with the hydrophobic self-assembled monolayer coating. e) EHDIJ printed TiO$_2$-PVP sink on Si wafer without the hydrophobic self-assembled monolayer coating. f) EHDIJ printed TiO$_2$-PVP sink on Si wafer with the hydrophobic self-assembled monolayer coating. g) Molecular diagram of TiO$_2$ precursor molecule. h) XRD of sintered (red) and unsintered (blue) TiO$_2$ precursor ink.

stage movement control and the printed feature size can be volumetrically varied on a drop-to-drop basis for single drop features in close proximity to each other.

Challenges for effective digital dropwise EHDIJ printing are the hysteretic effects associated with is the need to repeatedly start and stop the flow of ink. To achieve initial ink jetting, a higher nozzle electrode to ground plane potential difference is required to initiate droplet formation. This potential can be reduced once a droplet stream is established to achieve the smallest possible drop volume. There is a correlation between applied voltage and drop size, with the higher voltage resulting in larger ejected drops, thus increasing the size of the printed feature.[10] In dropwise mode, the EHDIJ printer needs to overcome this activation barrier energy at each feature

**ADVANCED
SCIENCE NEWS**
www.advancedsciencenews.com

**ADVANCED
MATERIALS
INTERFACES**
www.advmatinterfaces.de

location, therefore increasing the minimum feature size that can be achieved in this mode with respect to the continuous print mode. Continuous and dropwise printing methods were explored for this research and the highest resolution features were reported under both conditions.

Mid-infrared meta-optical lenses were printed using the dropwise mode in four sequential patterns, coinciding with the four different diameters (1–4 µm) of the meta-atoms present in the optimal infrared lensing design. The printer nozzle was kept at a uniform height (≈10 µm) throughout the printing process. The alternating current was applied in a 75% square waveform, which was uniform across the entire print. Each printed pattern was made with a different applied bias and wave amplitude, to modulate the printed feature size following the pattern of the designed meta-optics lens. The individual features of each pattern were printed in a single printing pass under one set of parameters; larger features were not achieved by printing in the same location with multiple drops. This is achieved by increasing the applied voltage between the nozzle and the stage to increase the volume of the ejected drop. If all other parameters remain constant, a larger applied voltage results in a larger ejected drop and thus a larger printed feature.

Post printing, the sample undergoes a thermal conversion step to enable crosslinking of the PVP and poly(melamine-co-formaldehyde) methylated, evaporate the printing solvents, and convert the titania precursor to amorphous TiO_2. Figure 1g shows the molecular structure of titanium diispropoxide bis(acetylacetonate), the titania precursor used in the printing solution. After the thermal crosslinking steps, the printed structures adhere well to the polished Si substrate, as tested through scratch testing and sonication in a solvent bath. Selected samples were exposed to an additional sintering step to convert the amorphous TiO_2 into anatase and burn off the residual PVP. Figure 1h shows the X-ray diffraction (XRD) spectra of the TiO_2 printing solution before and after the high-temperature annealing process. The diffraction peaks characteristic of the anatase phase of TiO_2 were detected in the samples after the high-temperature process, confirming the formation of crystalline TiO_2. XRD spectra from samples that did not undergo the annealing process were characteristic of an amorphous material.
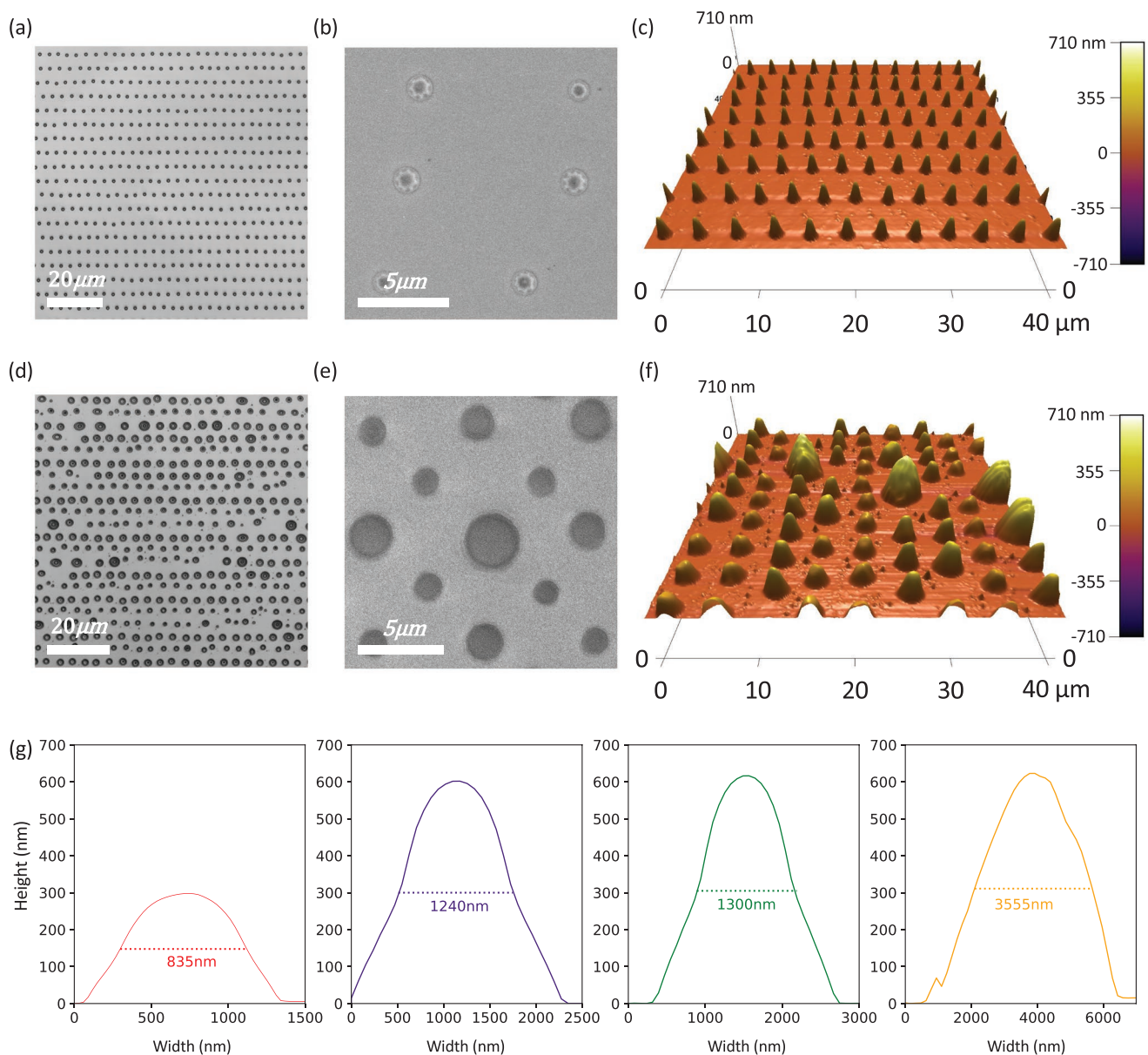
3. Results

The materials and process developed for this research resulted in the highest resolution EHDIJ printed TiO_2 reported in literature. The methods reported in this paper can be used to consistently print features on the order of 1 µm. **Figure 2**a shows an optical profilometry image and Figure 2b shows an SEM image of EHDIJ printed TiO_2 with an average feature diameter of 1.2 µm with the range of the printed features from 0.9 to 1.4 µm. The average height of the printed features in this array is 297 nm, as measured by AFM. This sample was printed using the continuous print mode with a printer bed speed of 2.0 mm s^{-1}. Figure 2d shows an optical profilometry image and Figure 2e shows an SEM image of EHDIJ printed TiO_2 printed using the dropwise print mode. This is an example of the range of features necessary to fabricate a meta-optics lens designed

to focus 5 µm light. The different feature sizes present in this example are intentional and were printed using different applied biases and wave frequencies. The range of features in this example lies between 1.2 and 6.0 µm, as measured at the base of the printed feature. The designed range of sizes for the features was 1.0 to 4.0 µm. Figure 2c,f shows AFM height images of the samples from Figure 2a,d respectively. Figure 2g shows four AFM cross-sections of features with different base diameters (1.2, 2.2, 3.1, and 6.0 µm). The maximum height of each printed feature is 297, 597, 616, and 622 nm, respectively. The full width at half maximum of these printed features is 835 nm, 1.24 µm, 1.30 µm, and 3.6 µm, respectively.

Once the materials, substrate surface, and EHDIJ printing processes were developed to provide droplet volume control and a lateral resolution of 1 µm for functional TiO_2, these techniques were applied to create a fully printed 1 mm × 1 mm mid-infrared meta-optics lens, based on discrete scattering features, designed to focus 5µm light. The designed 2D metasurface is made up of regions of features ranging from 1 to 4 µm in diameter with a 5 µm pitch between each feature, regardless of the feature diameter. The printed version of the meta-optics resulted in features ranging from 1.2 to 6.0 µm. The metasurface was printed using the dropwise mode and each feature was printed with a single drop of varying volume, rather than printing multiple drops of a uniform volume to increase feature size. The drop volume is varied by changing the applied bias between the nozzle tip and the stage. **Figure 3**a shows the as-designed metasurface lens with each color in the pattern representing a different scattering feature diameter. Figure 3b shows a final, fully printed meta-optics lens, indicating that there is a high fidelity between the designed pattern and the printed pattern. Close-up images show that there are distinct diameter differences between the features printed at each set of printing parameters, with the larger features resulting from the higher voltage and larger wave amplitude. The 1 µm and 2 µm feature regions have consistently discrete features. The 3 and 4 µm feature regions have some discrete features but also show a significant number of merged structures. This defect appears to occur more frequently in regions of the substrate where there is a higher concentration of 3 or 4 µm diameter structures. There is a variation among the printed features of all diameters but because the feature-to-feature pitch is set at 5 µm in the mid-infrared meta-optics lens, as the features get larger, the room for error without resulting in merged printing drops decreases.

There is a strong correlation between the size of the ejected printed drop and the voltage applied between the nozzle and the substrate stage. With all other printing parameters remaining constant, this ink shows an increase in drop volume as the applied voltage increases. This is demonstrated by an increase in the final observed printed feature size. For the metalens shown in Figure 3a,b, the features designed to be 1 µm in diameter were printed with an applied voltage of 65 V, and the 2, 3, and 4 µm diameter features were printed with an applied voltage of 77, 95, and 105 V, respectively. It is important to note that the trend of increasing voltage resulting in larger ejected ink drops is present across the many samples that were printed but it is not the case that one applied voltage will result in a specific drop size every time. For example, other
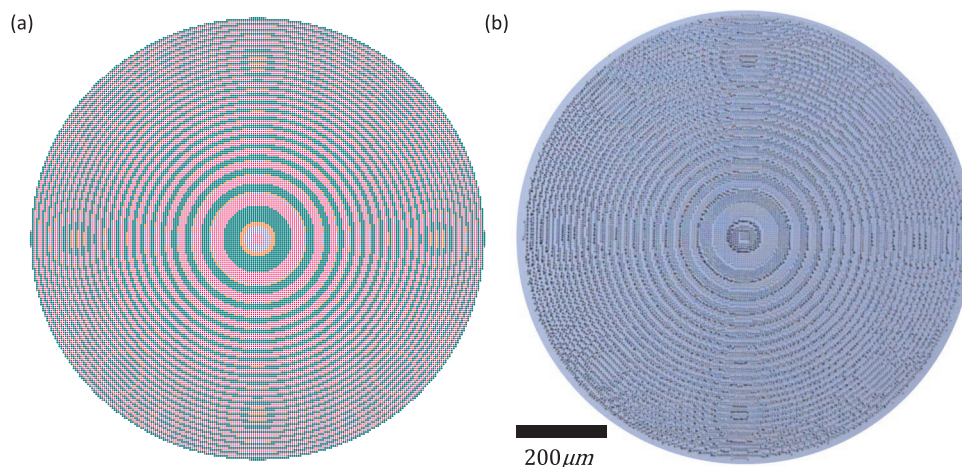
**ADVANCED
SCIENCE NEWS**

www.advancedsciencenews.com

**ADVANCED
MATERIALS
INTERFACES**

www.advmatinterfaces.de

Figure 2. a) Optical profilometry image of TiO$_2$ precursor ink printed in continuous EHDIJ mode, the scale bar is 20 µm. b) SEM image of TiO$_2$ precursor ink printed in continuous EHDIJ mode, the scale bar is 5 µm. c) AFM height scan image of samples shown in (a). d) Optical profilometry image of TiO$_2$ precursor ink printed in dropwise mode using different printing parameters for different sized features, the scale bar is 20 µm. e) SEM image of TiO$_2$ precursor ink printed in dropwise mode, the scale bar is 5 µm. f) AFM height scan image of samples shown in (d). g) Cross sections of printed features with four different sizes fabricated using different EHDIJ printing conditions showing the full width at half maximum height of the features.

metalenses were printed in a range of 88–210 V for the 1–4 µm diameter features. This difference in absolute applied voltage is likely due to other variables in the printing setup, such as small variations in nozzle height. Increasing and decreasing the nozzle height has been shown to impact the voltage required to initiate ink jetting. The further the nozzle is away from the substrate, the higher the applied voltage must be to create a large enough electric field to initiate ink jetting. Zhou et al. demonstrated the correlation between nozzle height, applied voltage, and feature size in a 2020 study where micron and submicron features of UV-curable polymers were printed

using the EHDIJ method.[10] The set-up used for the EHDIJ printed metalenses allows for top-down control of the nozzle distance away from the substrate with a movement resolution of 1 µm. However, this is not a dynamically controlled printing parameter and the nozzle height remains constant with respect to the top of the nozzle arm on the z-axis of the printer (see Figure 1a). Although these experiments were conducted in a climate-controlled laboratory with HEPA-filtered airflows, it is also possible that small variations in temperature, ambient relative humidity, stage roughness, and substrate and ink handling could lead to variations in the electric fields required for

**ADVANCED
SCIENCE NEWS**
www.advancedsciencenews.com

**ADVANCED
MATERIALS
INTERFACES**
www.advmatinterfaces.de

Figure 3. a) Designed mid-infrared metasurface lens. b) Optical profilometer image of fully printed mid-infrared meta-optics lens.

a given printing outcome. Therefore, it can be reported that a positive correlation exists between the applied voltage and the resulting printed drop volume but a precise quantitative relationship is presently unknown.

To validate the fabrication method, we designed a meta-optical lens, under the constraints of the printing fabrication. The phase-distribution $\Phi(x, y)$ of the metalens with a focal-length of f follows the hyperboloid phase profile:

$$\Phi(x, y) = \frac{2\pi}{\lambda}\left(\sqrt{x^2 + y^2 + f^2} - f\right) \tag{1}$$

For printable photonics, the highest achievable thickness of the scatter is ≈1 μm, under the current materials and methods, which limits the phase-coverage. Under the constraints of the printable features, we estimated the phase coverage to be ≈0.6 π, which is sufficient to create a lens.[24] **Figure 4**a shows the amplitude and phase distribution of the designed meta-optics lens.

We characterized the printed meta-optics using a confocal microscopy setup in mid-IR. In this microscope configuration, a pulsed 5 μm quantum cascade laser (QCL) with 500 ns pulses, and repetition rate of 100 kHz is coupled to an InF₃ single-mode fiber (NA ≈0.26 with 9 μm core) and collimated using a black diamond asphere (NA = 0.85) resulting in a collimated beam of ≈1 mm to match the metasurface clear aperture. The metasurface is translated relative to an imaging lens with a clear aperture of ≈25 mm and f = 12.7 mm. The image is captured on an InSb focal plane array (FPA) with a 15 μm pixel pitch and 640 × 512 pixels cooled to 76 K. The camera acquisition time is 0.9 ms to best fit the 14-bit dynamic range of the FPA and 100 frames are captured and averaged with background correction.

We clearly observe the focusing of the light as we scan along the optical axis (Figure 4c,d) and we can fit the intensity at the focal plane to estimate the FWHM of the beam spot to be ≈15 μm. We note that the focusing behavior is sub-optimal due to low phase coverage but the focusing behavior is expected to improve as we expand our printing capabilities and print thicker materials.

4. Discussion

The two main EHDIJ printing modes, as described previously, are the continuous printing mode and the dropwise printing mode. TiO₂ precursor metasurface printing trials for the 5 μm lens design revealed that the printing mode can significantly impact the printed feature resolution and feature shape. The highest resolution individually printed drops were consistently generated using continuous print mode. Discrete drops below 1 μm in diameter were consistently measured using the continuous print mode and the printed features had a more consistently uniform radius when compared to the dropwise printing method. The improved resolution using the continuous print mode could lead to fabricating devices to focus light with a wavelength smaller than 5 μm, thus expanding the applications for this printing method and the printed metasurface lenses.

The hydrophobic SAM (trichloro(1H, 1H, 2H, 2H-per-fluoroctyl)silane) used to coat the polished Si wafer is an essential process step to enable the high resolution features achieved in this study. Total wetting between the ink and the substrate is observed when the TiO₂ precursor solution is deposited on a clean and uncoated Si wafer. The contact angle increases to 68° with the addition of the hydrophobic SAM. In terms of film thickness, this translates to an increase in the single drop height from 20 nm on the uncoated Si to as tall as 620 nm on the hydrophobic SAM coated substrate. To optimally lens 5 μm light, the 1–4 μm diameter features should have a height of 1 μm. Lensing is still observable with a smaller feature height, but the results could be improved by printing higher aspect ratio features. One pathway to further increase feature height and aspect ratio is to use a different hydrophobic self-assembling monolayer as a surface treatment that results in a higher contact angle between the printing solution and substrate. N-Octadecyltrichlorosilane and 1H,1H,2H,2H-Perfluorodecyl-trichlorosilane, when coated on a substrate, show a higher contact angle between water and the substrate than the SAM used in this research.[25,26] Increasing the contact angle of the printed drop could result in a smaller diameter feature with a higher aspect ratio than the structures printed in this study.
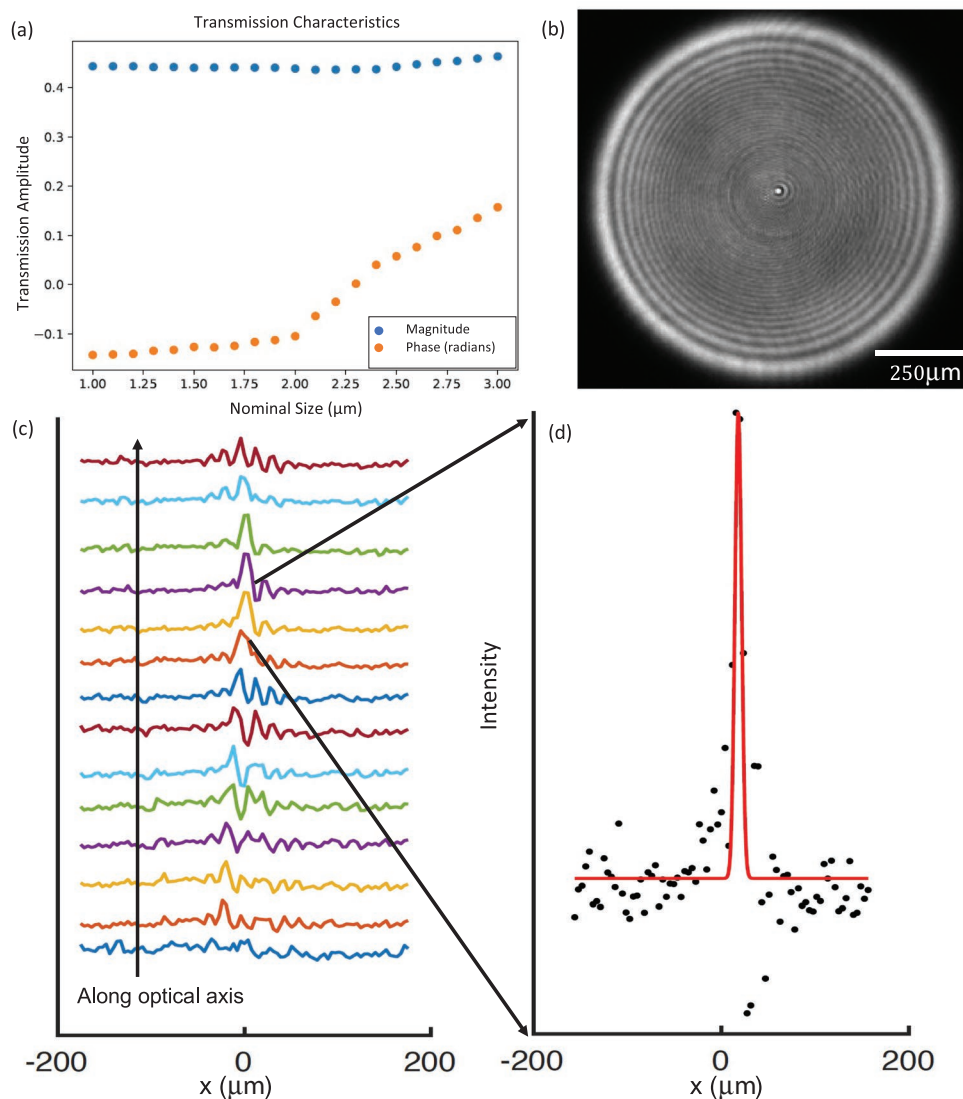
Figure 4. a) The amplitude and phase of the scatterer as a function of the scatterer diameter for light propagating perpendicular to the plane of the metasurface that is typically parallel to the long axis of the scatter feature. b) Signal intensity image showing the most power in the focal spot at the center. c) Focusing measurements taken along the optical axis. d) Peak intensity focusing measurement showing FWHM of the beam spot is $\approx$15 μm.

In addition to increasing the solution-substrate contact angle through changing the hydrophobic SAM coating, the printed feature aspect ratio could be increased through the addition of TiO_2 nanoparticles to form a composite nanoparticle and precursor ink. Metal nanoparticle and organic functional inks have been used to create very high aspect ratio features,[4] and a similar approach could be taken to increase the aspect ratio of EHDIJ printed TiO_2. The nanoparticles could enable higher aspect ratio features compared to particle-free inks, as well as an increase in viscosity of the printing solution, which can lead to less lateral droplet spreading before the solvent loss and increasing viscosity effectively freezes the droplets at their maximum lateral dimensions. The high melting temperature of oxides makes a solely nanoparticle-based printing solution undesirable, as the printed features are more likely to be discontinuous, porous, and adhere poorly to the substrate. However, combining the alkoxide precursor printing solutions, which

convert to crystalline TiO_2 at 450 °C, with TiO_2 nanoparticles could result in a printing solution that enables higher aspect ratio features from a given droplet volume while still being able to bind the nanoparticles together with TiO_2 and the substrate. It may also be possible to modify the spreading of printed droplets on the substrate through surfactants in the ink or printing a varying surface energy pattern on the substrate prior to the TiO_2 precursor deposition.

The addition of TiO_2 nanoparticles could also lead to an increase in the refractive index of the printed features. There is a positive correlation between an increasing refractive index and a reduction in the focal length of the measured metasurface lens, which is a device benefit for ultraflat optics.[15] At a wavelength of 5 μm, the effective refractive index of the printed TiO_2 structures is 1.9. This is lower than the refractive index of bulk TiO_2 at this wavelength, which is 2.24. One reason for the lower refractive index is due to the blend of PVP and TiO_2 in

the printed structures. During the high-temperature sintering process that is performed after printing, the PVP burns out and the remaining structures are converted to anatase. This results in some porosity in the TiO_2 with an effective refractive index proportional to the fractions of TiO_2 and void spaces that are below the refractive index of bulk TiO_2. The addition of TiO_2 nanoparticles could result in printed features with a higher ratio of TiO_2 to PVP as well as an overall higher solid loading of the precursor ink, leading to a higher effective refractive index with or without a high-temperature alkoxide conversion process and increased metasurface feature heights with the same lateral resolution. These factors are pathways toward improved EHDIJ printed metasurface lenses.

The performance of the metasurface is limited by the vertical height of the printable scatterer features, which limits the achievable phase coverage. Further increasing the aspect ratio of the printable film through ongoing ink materials, surface, and printing process parameter development will improve the phase coverage and efficiency.

5. Conclusion

In this study, a fully additive, maskless process for printing TiO_2 metasurface lenses made with femtoliter dropwise control of the printed ink features was developed. This technique was used to create mid-IR optical metasurface lenses that demonstrated focusing of 5 µm wavelength light. Two different EHDIJ printing modes, continuous and dropwise, were explored in an effort to create a minimum reproducible feature size of 1 µm. The dropwise method was used for the fully printed mid-infrared metasurface lens, as it allowed for the greatest control over material deposition location and local printed feature size. A TiO_2-PVP printing solution was designed specifically for this application to achieve higher aspect ratio features (1:2) with a refractive index approaching 2. Lensing of 5 µm light was observed at the designed focal depth of 1 µm. Although there are opportunities for further improvements in the printing materials and process to increase precision, printing consistency, feature aspect ratio, refractive index, and lensing efficiency, the reported results are the first of their kind both in the fields of printed meta-optics and EHDIJ printed ceramics.

6. Experimental Section

To make the printing solution, first, 0.625 g of PVP (≈55000 mw, Sigma-Aldrich) was added to a glass scintillation vial. Then 1.76 mL of EG (Reagent Plus > 99%, Sigma-Aldrich) and 0.638 mL of IPA (ACS Reagent > 99.5%, Sigma-Aldrich) were added to the vial. The PVP and solvents were stirred at room temperature, using a clean magnetic stir bar, at 600 rpm, until the PVP had fully dissolved, ≈2–3 h. Once the PVP was dissolved, 1.1125 g of titanium diisopropoxide bis(acetylacetonate) (75 wt.% solution in IPA, Sigma–Aldrich) and 0.125 g of poly(melamine-co-formaldehyde) methylated solution (≈84 wt.% in 1-butanol, Sigma–Aldrich) was added to the solution. The solution was stirred at room temperature for 24 h. Upon removing the sample from the stir plate after the 24 h of mixing was completed, the bulk solution was stored in air at room temperature. The final printing solution was made by taking 0.5 mL of the bulk solution and adding 0.5 mL of EG and 0.5 mL of titanium diisopropoxide

bis(acetylacetonate). This solution was mixed for 30 s using a vortex mixer at 2000 rpm. Just before printing, the final solution was filtered using a 0.45 µm, water-wetting polytetrafluoroethylene (PTFE) membrane syringe filter (VWR).

The 1 mm × 1 mm meta-optical lenses were fabricated on a commercially available, double side polished, n-type silicon wafer (University Wafer, Inc). The wafer was first cleaned via sonication baths in deionized (DI) water with 10% detergent, pure DI water, acetone, and IPA. Following sonication in IPA, the Si wafer undergoes a UV-ozone surface activation treatment for 10 min. Then the substrate was coated with trichloro(1H, 1H, 2H, 2H-perfluorooctyl)silane (97%, Sigma–Aldrich), a hydrophobic, self-assembling monolayer (SAM). The hydrophobic coating was applied in an enclosed environment on a hotplate set to 125 °C for 2 h. After the application of the hydrophobic monolayer, the metasurface was printed on the substrate using an electrohydrodynamic inkjet (EHDIJ) printer made by SIJ Technology. The nozzle used for printing the meta-optical lens was made of glass with an inner diameter of 2 µm. The nozzle has a thin gold filament that runs inside the glass nozzle, which connects to the conductive, top portion of the nozzle (Figure 1b). The nozzles were purchased from SIJ Technology and were commercially available. The samples were printed under ambient conditions with the printing nozzle kept at a uniform height (≈10 µm). This distance was measured by using the tool's z-axis digital nozzle control. First, the nozzle is brought close to the stage until it touches the substrate. Then, the nozzle was retracted by 10 µm. This distance was set at the origin of the printed region and the nozzle does not move in the z-axis while the pattern was printed. After printing the complete metasurface, the substrate was placed on a 200 °C hotplate for 20 min. This was to enable the thermal crosslinking of the PVP and poly(melamine-co-formaldehyde) methylated, to evaporate the printing solvents, and convert the titania precursor to amorphous TiO_2. Some samples were exposed to a high temperature process in order to convert the amorphous TiO_2 into the crystalline, anatase phase of TiO_2. During this step, the samples were heated in a box furnace to 450 °C and held at that temperature for 1 h. After thermal conversion of the ink, the samples were assessed for printing quality using an optical profilometer (Olympus OLS4100), SEM (FEI Sirion XL30 and FEI Apreo VP), and AFM (Oxford Instruments, Jupiter XR). Determination of the printed feature size was done using both the image analysis software in the AFM and with the image analysis software, Fiji. Material and phase analyses were conducted with XRD (Bruker D8 Advanced XRD).

Conflict of Interest

The authors declare no conflict of interest.

Data Availability Statement

The data that support the findings of this study are available from the corresponding author upon reasonable request.

Keywords

[1] J. Carter, P. Lyon, C. Creighton, M. Bale, H. Gregory, *SID Int. Symp. Dig. Tec.* **2005**, *36*, 523.

[2] S. Burns, C. Kuhn, K. Jacobs, J. D. MacKenzie, C. Ramsdale, A. C. Arias, J. D. Watts, M. Etchells, K. Chalmers, P. Devine, N. Murton, S. Norval, J. King, J. Mills, H. Sirringhaus, R. Friend, *J. Soc. Inf. Display* **2003**, *11*, 599.

[3] A. C. Arias, J. D. MacKenzie, I. McCulloch, J. Rivnay, A. Salleo, *Chem. Rev.* **2010**, *110*, 3.

[4] B. W. An, K. Kim, H. Lee, S. Kim, Y. Shim, D. Lee, J. Y. Song, J. Park, *Adv. Mater.* **2015**, *27*, 4322.

[5] B. Y. Ahn, E. B. Duoss, M. J. Motala, X. Guo, S. Park, Y. Xiong, J. Yoon, R. G. Nuzzo, J. A. Rogers, J. A. Lewis, *Science* **2009**, *323*, 1590.

[6] J. Park, M. Hardy, S. J. Kang, K. Barton, K. Adair, D. K. Mukhopadhyay, C. Y. Lee, M. S. Strano, A. G. Alleyne, J. G. Georgiadis, P. M. Ferreira, J. A. Rogers, *Nat. Mater.* **2007**, *6*, 782.

[7] B. Zhang, J. He, X. Li, F. Xu, D. Li, *Nanoscale* **2016**, *8*, 15376.

[8] J. Schneider, P. Rohner, P. Galliker, S. N. Raja, Y. Pan, M. K. Tiwari, D. Poulikakos, *Nanoscale* **2015**, *7*, 9510.

[9] H. Kwon, J. Hong, S. Y. Nam, H. H. Choi, X. Li, Y. J. Jeong, S. H. Kim, *Materials* **2021**, *2*, 5593.

[10] P. Zhou, H. Yu, W. Zou, Y. Zhong, X. Wang, Z. Wang, L. Liu, *Opt. Express* **2020**, *28*, 6336.

[11] H. T. Yudistira, A. P. Tenggara, S. S. Oh, V. Nguyen, M. Choi, C.-g. Choi, D. Byun, *J. Micromech. Microeng.* **2015**, *25*, 045006.

[12] T. T. T. Can, T. C. Nguyen, W.-S. Choi, *Adv. Eng. Mat* **2020**, *22*, 1901384.

[13] S. M. Kamali, E. Arbabi, A. Arbabi, A. Faraon, *Nanophotonics* **2018**, *7*, 1041.

[14] Y. Kivshar, *Nat. Sci. Rev.* **2018**, *5*, 144.

[15] E. Bayati, A. Zhan, S. Colburn, M. V. Zhelyeznyakov, A. Majumdar, *Appl. Optics* **2019**, *58*, 1460.

[16] D. Wen, F. Yue, W. Liu, S. Chen, X. Chen, *Adv. Opt. Mater.* **2018**, *6*, 1800348.

[17] J. Muller, *Microsyst. Technol.* **2003**, *9*, 308.

[18] E. B. Duoss, M. Twardowski, J. A. Lewis, *Adv. Mater.* **2007**, *19*, 3485.

[19] A. Zhan, S. Colburn, R. Trivedi, T. K. Fryett, C. M. Dodson, A. Majumdar, *ACS Photonics* **2016**, *3*, 209.

[20] L. Huang, S. Colburn, A. Zhan, A. Majumdar, *Adv. Photonics Res.* **2022**, 2100265.

[21] J. Engelberg, U. Levy, *Nature Commun* **2020**, *11*, 1991.

[22] R. Paniagua-Dominguez, Y. F. Yu, E. Khaidarov, S. Choi, V. Leong, R. M. Bakker, X. Liang, Y. H. Fu, V. Valuckas, L. A. Krivitsky, A. I. Kuzentsov, *Nano Lett.* **2018**, *18*, 2124.

[23] P. Zhou, H. Yu, Y. Zhong, W. Zou, Z. Wang, L. Liu, *Nano-Micro Lett.* **2020**, *12*, 166.

[24] C.-H. Liu, J. Zheng, S. Colburn, T. K. Fryett, Y. Chen, X. Xu, A. Majumdar, *Nano Lett.* **2018**, *18*, 6961.

[25] D. Janssen, R. De Palma, S. Verlaak, P. Heremans, W. Dehaen, *Thin Solid Films* **2006**, *515*, 1433.

[26] M. Psarski, G. Celichowski, E. Bystrzycka, D. Pawlak, J. Grobelny, M. Cichomski, *Mater. Chem. Phys.* **2018**, *204*, 305.